26. Ratnieks, F. L. W. & Visscher, P. K. Worker policing in the honeybee. *Nature* **342,** 796–797 (1989).
27. Barron, A., Oldroyd, B. P. & Ratnieks, F. L. W. Worker reproduction in honey-bees (*Apis*) and the anarchic syndrome: a review. *Behav. Ecol. Sociobiol.* **50,** 199–208 (2001).
28. Foster, K. R. & Ratnieks, F. L. W. Social insects: Facultative worker policing in a wasp. *Nature* **407,** 692–693 (2000).
29. Foster, K. R. & Ratnieks, F. L. W. Convergent evolution of worker policing by egg eating in the honeybee and common wasp. *Proc. R. Soc. Lond. B* **268,** 169–174 (2001).
30. Peeters, C., Monnin, T. & Malosse, C. Cuticular hydrocarbons correlated with reproductive status in a queenless ant. *Proc. R. Soc. Lond. B* **266,** 1323–1327 (1999).

Acknowledgements

We thank IBAMA for permission to collect *Dinoponera* in Brazil, and T. Clutton-Brock, M. Cobb, K. Foster, A. Hefetz, L. Keller, J. Liebig and C. Peeters for comments. T.M. was funded by a Marie Curie individual fellowship from the European Union programme Training and Mobility of Researchers.

Competing interests statement

The authors declare that they have no competing financial interests.

Correspondence and requests for materials should be addressed to T.M. (e-mail: Thibaud.Monnin@snv.jussieu.fr).

An ultra-sparse code underlies the generation of neural sequences in a songbird

Richard H. R. Hahnloser*†‡, Alexay A. Kozhevnikov*‡ & Michale S. Fee*

* *Biological Computation Research Department, Bell Laboratories, Lucent Technologies, Murray Hill, New Jersey 07974, USA*
† *Howard Hughes Medical Institute, Department of Brain and Cognitive Sciences, Massachusetts Institute of Technology, Cambridge, Massachusetts 02139, USA*
‡ *These authors contributed equally to this work*

Sequences of motor activity are encoded in many vertebrate brains by complex spatio-temporal patterns of neural activity; however, the neural circuit mechanisms underlying the generation of these pre-motor patterns are poorly understood. In songbirds, one prominent site of pre-motor activity is the forebrain robust nucleus of the archistriatum (RA), which generates stereotyped sequences of spike bursts during song[1] and recapitulates these sequences during sleep[2]. We show that the stereotyped sequences in RA are driven from nucleus HVC (high vocal centre), the principal pre-motor input to RA[3,4]. Recordings of identified HVC neurons in sleeping and singing birds show that individual HVC neurons projecting onto RA neurons produce bursts sparsely, at a single, precise time during the RA sequence. These HVC neurons burst sequentially with respect to one another. We suggest that at each time in the RA sequence, the ensemble of active RA neurons is driven by a subpopulation of RA-projecting HVC neurons that is active only at that time. As a population, these HVC neurons may form an explicit representation of time in the sequence. Such a sparse representation, a temporal analogue of the 'grandmother cell'[5] concept for object recognition, eliminates the problem of temporal interference during sequence generation and learning attributed to more distributed representations[6,7].

Songbirds produce highly stereotyped, learned vocalizations[8,9]. Zebra finch (*Taeniopygia guttata*) song consists of a complex pattern of sounds with spectral and temporal modulation over a wide range of timescales[10]. A basic acoustic element is the song syllable, which may itself be composed of a complex sequence of sounds varying on a 10-ms timescale, or even less[11]. Several distinct song syllables are organized into a single, repeated pattern of about 1 s in duration, called a song motif. Two pre-motor nuclei have been identified for their importance in song generation: nucleus RA and nucleus HVC[12]. Premotor HVC neurons project onto RA neurons, which in turn project with a myotopic mapping onto motor neurons of the vocal organ[13], and to respiratory brain areas[14]. During singing, RA neurons generate a highly stereotyped, complex sequence of action potential bursts, each precisely correlated to the song vocalization on a submillisecond timescale[1,15]. The average burst duration is roughly 10 ms, and each RA neuron generates a unique pattern of roughly ten bursts per song motif, such that on average 12% of RA neurons are active at any time (A. Leonardo, and M.S.F., unpublished data) (Fig. 1a).

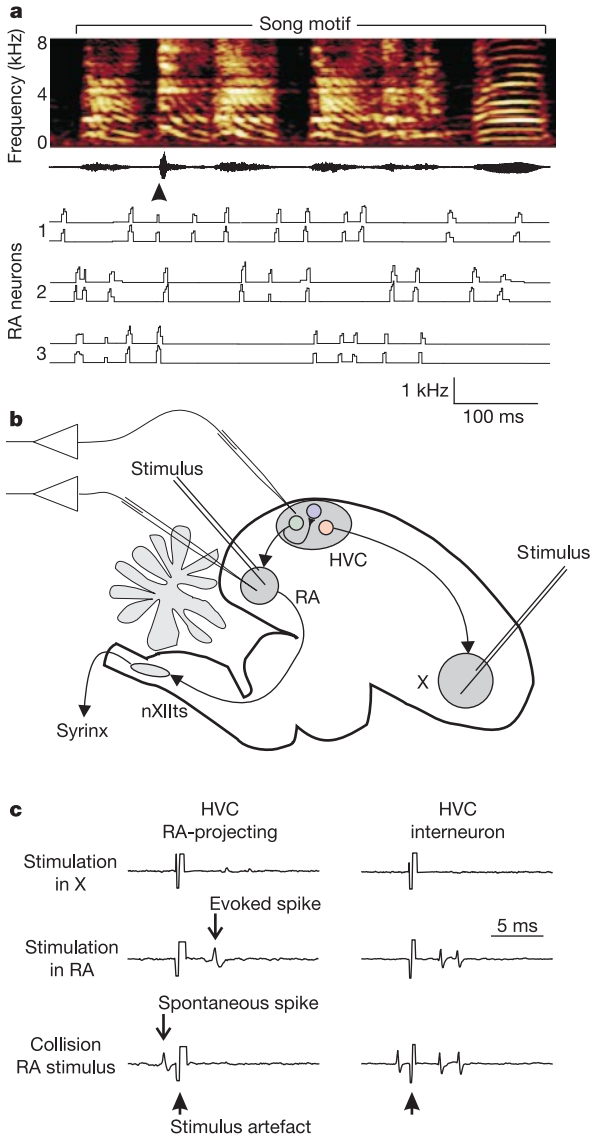

Figure 1 RA sequences and identification of HVC neurons. **a**, Neurons in nucleus RA generate complex sequences of brief action potential bursts during song vocalizations. Spectrogram (top) and acoustic signal of the song motif, and plots of instantaneous firing rate (bottom) of song-related spike activity in three different RA neurons recorded in one zebra finch. Neural activity is aligned using the onset of the second syllable of each motif (arrowhead). Two renditions are displayed for each neuron. **b**, Single-unit recordings were made in pre-motor nuclei HVC and RA. HVC neurons were antidromically identified by electrical stimulation in RA and area X. RA projects to vocal motor neurons in the nucleus of the twelfth nerve (nXIIts). **c**, RA-projecting neurons and putative interneurons could be activated from RA but not from area X. Stimulation in RA, triggered by spontaneous spikes, resulted in spike collision for RA-projecting neurons but not for interneurons.

Here, we avoid the question of how RA activity is translated into sound, and simply ask how pre-motor burst patterns in RA are generated. Previous studies have suggested that the syllable order and tempo of the motif are generated by a network that resides above RA, and includes HVC[12,16], and that an HVC neural code for syllables is transformed into a code for shorter acoustic elements through the projection of HVC onto RA[1,17]. To re-examine these issues, we have characterized the role of inputs to RA from pre-motor nucleus HVC.

HVC contains at least three classes of neurons: neurons that project to the RA, neurons that project to area X, and interneurons[18,19]. We have identified HVC neuron classes by antidromic activation[20] from RA and from area X (Fig. 1b, c). Chronic single-neuron recordings were made from identified neurons of all three classes. Antidromically identified RA-projecting HVC neurons ($HVC_{(RA)}$) ($n = 16$, three birds) were completely inactive in awake, non-singing birds (<0.001 spikes s^{-1}), and burst extremely sparsely during vocalizations, generating at most a single burst per song motif (Fig. 2a). $HVC_{(RA)}$ bursts had a duration of 6.1 ± 2 ms, and comprised 4.5 ± 2 spikes at a firing rate of $613 \pm 210\ s^{-1}$ (ranges are ± 1 s.d. unless specified otherwise). $HVC_{(RA)}$ bursts were highly stereotyped, tightly time-locked to the song motif (0.66 ± 0.14 ms r.m.s. jitter), and occurred reliably on every rendition of the motif (Fig. 2b). Thus, on a millisecond timescale, $HVC_{(RA)}$ bursts were maximally correlated to the vocalization. Different $HVC_{(RA)}$ neurons tended to burst at different times in the song, with no obvious timing relation to the onset or offset of song syllables. Three identified $HVC_{(RA)}$ neurons generated no bursts during the song, but produced a single burst during call vocalizations. HVC neurons projecting to area X also burst sparsely during singing (0–5 bursts per motif, $n = 30$; data not shown). In contrast to projection neurons, putative HVC interneurons ($n = 31$), most of which were spontaneously active in the non-singing bird (11 ± 7 spikes s^{-1}), produced high rates of spiking and bursting activity throughout song and call vocalizations (Fig. 2b). The firing patterns of putative HVC interneurons were similar to those of unidentified neurons found in previous studies of HVC in the singing bird[1].

Previous observations have shown that sleep-related spike and burst patterns in nucleus RA can closely recapitulate those generated during singing[2], suggesting that a common neural mechanism may underlie the generation of song- and sleep-related RA burst patterns. A more detailed understanding of the role of HVC in generating sleep-related activity in RA may provide a hint as to the interaction of these two nuclei during singing. We next examined the firing patterns of RA neurons and identified HVC neurons using a new, sleeping-bird preparation where the head of the bird is fixed, permitting simultaneous single-unit recordings in multiple brain areas and pharmacological manipulation, which are not currently possible in the singing bird.

Similar to the situation in the singing bird, $HVC_{(RA)}$ neurons burst sparsely during sleep (0.06 ± 0.05 bursts s^{-1}, $n = 116$, 27 birds). Paired recordings in RA and HVC (Fig. 3a) neurons showed that $HVC_{(RA)}$ neurons fired 13 ± 3 times fewer bursts in the sleeping bird than did RA neurons ($n = 53$ pairs). The bursts had properties similar to those observed during singing: duration of bursts during sleep in RA and $HVC_{(RA)}$ neurons were 11.5 ± 3.5 ms and 6.5 ± 1.8 ms, respectively. Bursts of $HVC_{(RA)}$ neurons during sleep comprised 3.2 ± 0.8 spikes per burst, and had an average firing rate of $347 \pm 81\ s^{-1}$. The relationship between $HVC_{(RA)}$ bursts and RA bursts is readily seen in raster plots of RA spike trains aligned in time to the onset of bursts in $HVC_{(RA)}$ neurons (Fig. 3b, c). RA neurons reliably showed a pattern of bursts locked to the $HVC_{(RA)}$ bursts ($n = 45$ of 53 pairs). Furthermore, multiple RA neurons recorded sequentially with a single $HVC_{(RA)}$ neuron ($n = 3$) show that different RA neurons generate different patterns of bursts, as is the case during singing. The relation between $HVC_{(RA)}$ and RA spike trains was quantified using a correlation

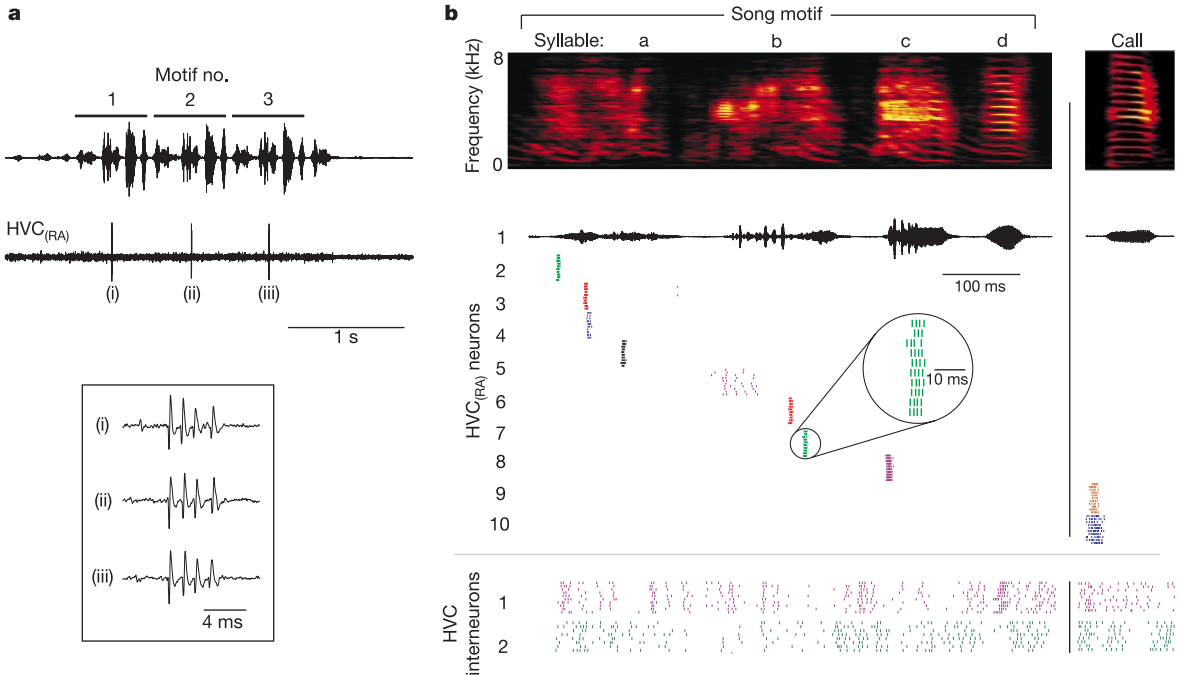

Figure 2 Spiking activity of identified HVC neurons during singing. **a**, Extracellular record of an RA-projecting HVC ($HVC_{(RA)}$) neuron (bottom), with the simultaneously recorded vocalization (top). The $HVC_{(RA)}$ neuron generates a single burst during each of three motif renditions. **b**, Spike raster plot of ten $HVC_{(RA)}$ neurons and two HVC interneurons recorded in one bird during singing (left) and call vocalizations (right). Each row of tick marks shows spikes generated during one rendition of the song or call; roughly ten renditions are shown for each neuron. Neural activity is aligned by the acoustic onset of the nearest syllable. $HVC_{(RA)}$ neurons burst reliably at a single precise time in the song or call; however, HVC interneurons spike or burst densely throughout the vocalizations.

function, $K(\tau)$, that is conditional on spikes in the $HVC_{(RA)}$ neuron ($-1 < K(\tau) < 1$) (ref. 21) (see Methods). Unlike the standard cross-correlation function, $K(\tau)$ is not sensitive to large differences in firing rate of the two spike trains. The peaks in the conditional correlation function in RA–$HVC_{(RA)}$ pairs were large; the largest peak correlation for each pair was on average $\bar{K} = 0.62$ ($n = 45$ pairs). Multiple significant peaks in $K(\tau)$, corresponding to reliable bursts in the RA sequence, were found over a wide range of time lags (±400 ms full range, ±130 ms s.d.), with weaker correlations at larger time lags (Fig. 3d). Significant peaks were approximately symmetrically distributed around zero time lag; that is, bursts in the RA sequence were observed both before and after the $HVC_{(RA)}$ bursts.

Paired recordings of $HVC_{(RA)}$ neurons reveal that these neurons generate a sparse sequence during sleep (Fig. 3e), consistent with our observations in the singing bird. Nine $HVC_{(RA)}$ pairs (out of 26 pairs, 7 birds) showed a statistically significant conditional correlation; in only one of these pairs did the neurons burst simultaneously. The time lags of the peaks were distributed over several hundred milliseconds (Fig. 3f), showing that the population of $HVC_{(RA)}$ neurons forms a sequence over a timescale similar to that of the sleep sequences in RA neurons. $HVC_{(RA)}$ pairs recorded on a single electrode revealed that neighbouring $HVC_{(RA)}$ neurons did not burst at the same time ($n = 3$ in the sleeping bird, $n = 1$ in the singing bird), suggesting that there may be no spatial organization to the burst times in HVC.

In the singing bird, $HVC_{(RA)}$ neurons burst at most once per motif, thus spike train autocorrelations of these neurons do not exhibit any peaks at time lags greater than 10 ms and less than the motif duration. Similarly, the autocorrelations of $HVC_{(RA)}$ neurons recorded during sleep did not show significant peaks at time lags greater than 10 ms (134 of 135 neurons). Furthermore, during singing, pairs of $HVC_{(RA)}$ neurons are highly correlated at a single time lag corresponding to the interval between their burst times in the motif (as inferred from their correlation to the vocalization, see Fig. 2). Similarly, during sleep, correlated $HVC_{(RA)}$ pairs show only a single significant peak in the conditional correlation function (for 8 of 9 correlated pairs, Fig. 3f).

Do action potential bursts in $HVC_{(RA)}$ neurons drive bursts in RA neurons? Reversible lesions in HVC demonstrate that spiking activity in HVC is necessary for the generation of sleep sequences in RA. In three birds, microinjection into HVC of lidocaine, a sodium channel blocker that suppresses spiking, completely and reversibly abolished sleep bursts in RA. Total recovery was observed 2–3 min after injection. Injections in HVC had no effect on the spontaneous 10–20-Hz regular spiking in RA neurons, confirming that lidocaine did not diffuse into RA. Control injections of saline had no effect on sleep bursts ($n = 3$ birds). Injections of lidocaine into forebrain nucleus LMAN[22], a non-pre-motor input to RA, did not affect the generation of bursts during sleep ($n = 2$ birds).

Evidence that bursts in RA are driven in a feed-forward manner by preceding activity in the HVC is also provided by observations of

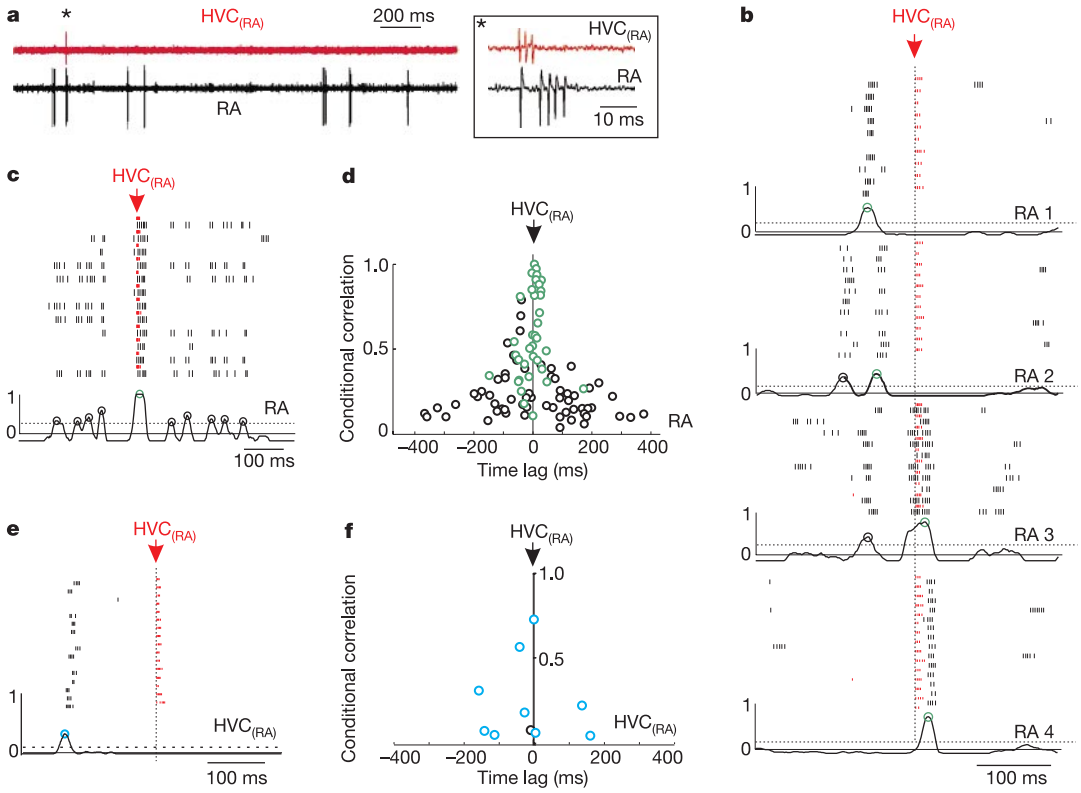

Figure 3 Relationship between burst patterns in a sleeping bird of RA neurons and $HVC_{(RA)}$ neurons. **a**, Extracellular signals from an $HVC_{(RA)}$ neuron recorded simultaneously with an RA neuron. $HVC_{(RA)}$ neurons burst sparsely, approximately 13 times less often than RA neurons. **b**, Spike raster plot of simultaneously recorded pairs of $HVC_{(RA)}$ and RA neurons. Shown is one $HVC_{(RA)}$ neuron recorded sequentially with four different RA neurons. All $HVC_{(RA)}$ bursts (short red rasters) are aligned at the centre of the plot. Corresponding RA spikes (long black rasters) are shown below each $HVC_{(RA)}$ burst. Below each raster is shown the conditional correlation function. **c**, Another example of an RA burst sequence in a sleeping bird (without melatonin). Green circles show the largest statistically significant correlation peak; black circles show statistically significant secondary peaks. The horizontal dashed line is the 95% confidence level, as assessed by Monte-Carlo estimation. **d**, Distribution of peak correlation and time lag of statistically significant main peaks (green) and secondary peaks (black). Positive time indicates that the RA neuron follows the $HVC_{(RA)}$ neuron. **e**, Raster plot of simultaneously recorded $HVC_{(RA)}$ neurons, with conditional correlation function below. **f**, Peak values and associated time lags of the conditional correlation functions for $HVC_{(RA)}$ pairs (blue circles show significant main peaks ($P < 0.05$), the black circle shows the only secondary peak).

putative HVC interneurons ($HVC_{(i)}$) in the sleeping bird. Paired recordings showed that the burst density of $HVC_{(i)}$ neurons was roughly three times the burst density of simultaneously recorded RA neurons ($n = 35$ pairs) and 45 times that of $HVC_{(RA)}$ neurons ($n = 22$ pairs). Bursts of $HVC_{(RA)}$ neurons were strongly synchronized with bursts of $HVC_{(i)}$ neurons (Fig. 4a; average correlation $\bar{K} = 0.73$, average latency $\tau = 2.5 \pm 3.0$ ms ($\pm$s.e.m.)). Similarly, most bursts of RA neurons strongly correlated with preceding bursts of $HVC_{(i)}$ neurons (Fig. 4a, c; average correlation $\bar{K} = 0.51$, average latency $\tau = 4.5 \pm 0.4$ ms ($\pm$s.e.m.)). The average spike latencies of RA and $HVC_{(RA)}$ neurons relative to $HVC_{(i)}$ neurons are consistent with the measured distribution of antidromic $HVC_{(RA)}$ spike latencies (3.5 ± 2.5 ms ($\pm$s.d.)). Because there is no known direct anatomical projection from RA to HVC, these results, together with the HVC lesion experiments, imply a short timescale ($\sim$4.5 ms) and causal relationship between $HVC_{(RA)}$ bursts and RA bursts.

The strong correlation between $HVC_{(RA)}$ and $HVC_{(i)}$ neurons suggests that activity in single $HVC_{(i)}$ neurons during sleep is representative of the population activity of $HVC_{(RA)}$ neurons. Consistent with this idea, all interneurons we observed were strongly activated by near-threshold antidromic stimulation of $HVC_{(RA)}$ neurons; additionally HVC interneurons were highly synchronized as a population during sleep (Fig. 4b). In paired recordings, nearly every sleep burst in one $HVC_{(i)}$ neuron occurred simultaneously with a burst in the other $HVC_{(i)}$ neuron ($\bar{K} = 0.78$, $n = 19$ pairs; Fig. 4c). Thus, the fact that bursts in $HVC_{(i)}$ neurons precede most sleep bursts in RA suggests that feed-forward activation from HVC dominates the generation of sleep sequences in RA. The feed-forward contribution, that is, the fraction of RA bursts that are driven from HVC, is given to a first approximation by the ratio of the RA–$HVC_{(i)}$ conditional correlation to the $HVC_{(RA)}$–$HVC_{(i)}$ conditional correlation. (The $HVC_{(RA)}$–$HVC_{(i)}$ conditional correlation is a measure of how well the $HVC_{(i)}$ neurons represent activity in the $HVC_{(RA)}$ population, and is therefore used as a normalization.) Thus, our estimate of the HVC feed-forward contribution to RA sleep sequences is 70%.

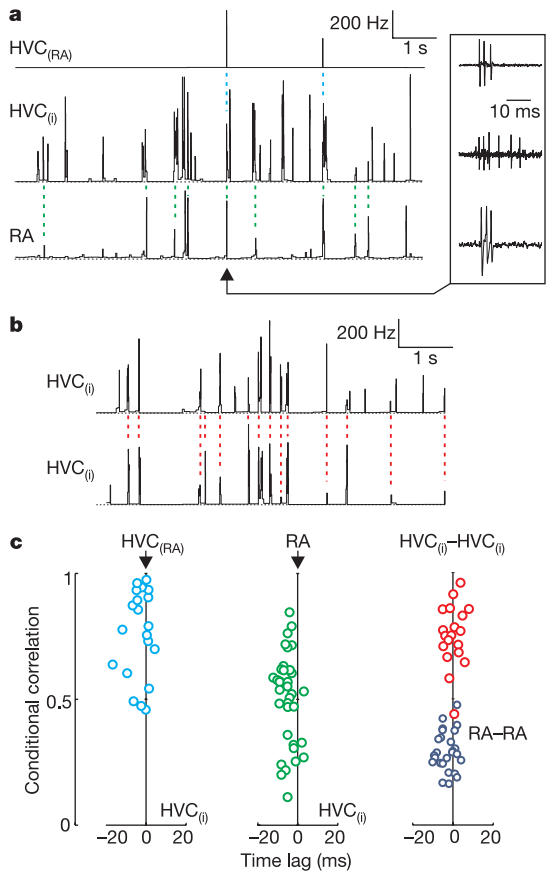

Figure 4 Global synchrony of HVC interneurons. **a**, Simultaneous single-unit triplet recording, during sleep, of an $HVC_{(RA)}$ neuron, a putative HVC interneuron ($HVC_{(i)}$) and an RA neuron. Plotted are instantaneous firing rate functions. RA bursts and $HVC_{(RA)}$ bursts are strongly synchronized with interneuron bursts. **b**, Instantaneous firing rate function for a simultaneously recorded pair of $HVC_{(i)}$ neurons, which show highly synchronized bursts. **c**, Scatter plot of conditional correlation versus peak times of 20 $HVC_{(RA)}$–$HVC_{(i)}$ pairs, 35 RA–$HVC_{(i)}$ pairs, 19 $HVC_{(i)}$–$HVC_{(i)}$ pairs, and 27 RA–RA pairs. For the left two plots, the time lag is plotted relative to the bursts of the $HVC_{(RA)}$ neuron and the RA neuron, respectively.

To what extent does this and other observations in the sleeping bird inform our understanding of the generation of RA song sequences? Are sleep sequences a transient activation of the same neural mechanisms that underlie the generation of sequences during singing? Previous studies indicate that during sleep, individual RA neurons can generate the same unique sequence of spikes and bursts as generated by that neuron during singing[2]. Our data do not allow a comparison of individual RA–$HVC_{(RA)}$ pair correlations in the sleeping and singing bird; however, we can compare RA and HVC correlations on a population basis in these two states. Although average correlations are weaker for sleep sequences, they share the following features with song sequences: (1) $HVC_{(RA)}$ neurons, as a population, generate sparse sequences; (2) most RA neurons generate a unique pattern of bursts in relation to a given $HVC_{(RA)}$ neuron burst; (3) the burst widths, and the ratio of burst densities of RA and $HVC_{(RA)}$ neurons are similar in both behavioural states; and (4) HVC interneurons fire or burst densely during both song and sleep sequences. In conclusion, the relationship between song and sleep sequences of individual neurons is unresolved, but our results suggest that the generation of RA song sequences may also be dominated by a feed-forward drive from HVC; that is, most of the RA bursts during singing are driven directly by bursts in $HVC_{(RA)}$ neurons.

Our finding that $HVC_{(RA)}$ neurons produce a brief burst at a single time in only one of the repeating vocal elements (that is, motif or call), and that, as a population, $HVC_{(RA)}$ neurons are probably active throughout the associated RA sequences, suggests that these neurons code for some transient event or 'state' in the sequence, rather than longer timescale structures such as song syllables, as was previously believed. We propose that $HVC_{(RA)}$ neurons code for a unique time within the RA sequence; that is, that they are active at one and only one time point in the RA sequence, regardless of motor or vocal content. This does not imply that $HVC_{(RA)}$ neurons can never burst more than once in a song motif: an $HVC_{(RA)}$ neuron active within a syllable identically repeated in a motif will probably burst during each repeat of the syllable, as suggested by the precisely repeated RA sequence associated with identical syllables within a motif[1] (A. Leonardo and M.S.F., unpublished observations). Given the precise relationship between $HVC_{(RA)}$ bursts and RA burst patterns however, it seems unlikely that $HVC_{(RA)}$ neurons will burst several times within a motif that does not have repeated RA, and therefore acoustic, sequences.

In most neural models of sequence generation, a sequence of activity is stored by specific excitatory and inhibitory connections between neurons within the network, such that the network advances autonomously from one state to the next[23,24]. Such single-layer recurrent networks suffer from the problem of temporal interference due to spatial overlap of different states in the sequence, and consequently must operate with very low average activity[6,7], cannot produce the same state at multiple times during the sequence, or are difficult to train[25]. The previous theoretical work showed that a sparse representation, such as we observe in HVC, resolves these interference problems. Our data indicate that the dynamics that underlie RA sequence generation occur not in RA but in another network (for example, the HVC and higher) that

incorporates a canonical sparse representation. The canonical sequence in HVC is translated into a complex sequence in RA by a set of synaptic weights from $HVC_{(RA)}$ to RA neurons; thus RA can, in principle, produce arbitrary sequences with high average levels of activity and large state overlaps.

Put in terms of songbird behaviour, the motor actions underlying song unfold when the 'time code' in HVC acts on the 'muscle map' in RA. The pattern of activation in RA depends on the synaptic connections from $HVC_{(RA)}$ neurons onto RA neurons, suggesting that it is the pattern of $HVC_{(RA)}$–RA synapses that contains the 'score' of the bird's song. Our results are thus consistent with the idea that plasticity in RA mediates song learning[26–28], and suggest that the site of this plasticity is the $HVC_{(RA)}$–RA synapse. Of course we cannot exclude the possibility that song learning may also involve plasticity in the order in which $HVC_{(RA)}$ neurons burst.

The ultimately sparse, or unary, representation in HVC may simplify sequence learning as well: errors in the song at a particular time in the sequence can be corrected, through auditory feedback, by altering only those $HVC_{(RA)}$–RA synapses that were active at the time of, or immediately preceding, the error. In a dense representation, in which $HVC_{(RA)}$ neurons would burst many times, changes in synaptic connectivity intended to reduce song errors at one time would affect song output at many times, resulting in a difficult learning process. However, with a sparse representation in HVC, changes in the $HVC_{(RA)}$–RA synapses during learning will modify the RA pattern, and thus the song, only at the time of the error, without introducing unwanted changes in the song at other times. □

Methods

Electrophysiology

Subjects were adult male zebra finches. The care and experimental manipulation of the animals was carried out in accordance with guidelines of the National Institute of Health and have been reviewed and approved by the local Institutional Animal Care and Use Committee. Before surgery, anaesthesia was produced with 1–3% isofluorane in oxygen. For experiments on sleeping birds, a thin stainless-steel plate was mounted to the skull with dental acrylic, and a window was made in the inner and outer bone leaflet over nuclei RA, HVC and area X of the right hemisphere using stereotaxic coordinates. A small hole (~200 μm) was made in the dura over each area and the exposed brain was protected with 2% low melting agarose in saline. Wound margins were treated with lidocaine gel. The animal was placed in a small foam restraint and placed in the recording apparatus without further anaesthesia. Birds that did not sleep spontaneously were administered subcutaneously 10 μg melatonin (Sigma) in phosphate buffered saline[29]. Additional details on assessing sleep state are described in the Supplementary Information. For experiments in the singing bird, single-unit recordings were made with a three-channel motorized microdrive, using previously described techniques[30]. For chronic and head-fixed HVC recordings, stimulating electrodes were implanted in RA and area X for antidromic activation of HVC. Data were obtained from 41 zebra finches.

In the sleeping bird, simultaneous paired and triplet single-neuron recordings were made in nucleus RA and HVC. In the singing bird, single neurons were recorded in HVC or in RA. High signal-to-noise (greater than 5:1) recordings were made with sharp glass and platinum/tungsten microelectrodes. All spike trains were confirmed to be single-unit by complete suppression of the spike autocorrelation functions at times less than 1 ms. Antidromic identification of HVC neuron type was based on spike collision and spike latency variability[20], as described in Supplementary Information.

After each experiment, the animal was killed by intraperitoneal injection of 20% urethane (300 μl). The brain was removed for histological examination of unstained slices to verify the location of stimulating and recording electrodes, and drug injection sites.

Data analysis

In Figs 1 and 4, neural activities are represented as instantaneous firing rates, $R(t)$, defined at each time as the inverse of the enclosed interspike interval, $R(t) = 1/(t_{i+1} - t_i)$, for $t_i < t \leq t_{i+1}$, where t_i is the time of the ith spike. A burst is defined as the interval over which the instantaneous firing rate exceeds 100 Hz. The burst rate is defined as the number of events per unit time in which the instantaneous firing rate crosses the 100-Hz threshold from below.

We use a measure of correlation between two simultaneously recorded spike trains, A and B, which is conditional on the spike train with fewer spikes. This measure is insensitive to differences in average firing rate. The conditional correlation function, $K(\tau)$, represents the excess fraction of spikes in train A that fall within a window $(\tau - \Delta t, \tau + \Delta t)$ of a spike in train B, where Δt is the half-width of the window. The spike times of A and B are denoted by $t_i^A (1 \leq i \leq N^A)$ and $t_j^B (1 \leq j \leq N^B)$, respectively, where A has a smaller number of spikes than B ($N^A < N^B$). In calculating the conditional correlation, we define the conditional spike probability, $c(\tau)$ (ref. 21), as the fraction of spikes in A that are within Δt of at least one spike in B. $c(\tau)$ is calculated as a function of an arbitrary time shift, τ, between the two spike trains. Thus,

$$c(\tau) = \frac{1}{N^A} \sum_i^{N^A} \Theta[\Delta t - \min_j(|t_i^A - t_j^B - \tau|)]$$

where $\Theta[x]$ is the Heavyside function: $\Theta[x] = 0$ if $x < 0$ and $\Theta[x] = 1$ otherwise. Note that $0 \leq c(\tau) \leq 1$.

The conditional correlation is defined as: $K(\tau) = (c(\tau) - \bar{c})/(1 - \bar{c})$, for $\bar{c} \leq 0.5$ where $\bar{c} = \langle c(\tau) \rangle_\tau$ denotes the average conditional spike probability calculated on randomly shifted spike trains, as described below. The conditional correlation characterizes the two spike trains as being somewhere between anti-correlated ($K = -1$) and strongly correlated ($K = 1$), and obeys the inequalities $-1 \leq -\bar{c}/(1 - \bar{c}) \leq K \leq 1$. Apart from normalization, the shape of the conditional correlation function is qualitatively similar to the standard cross-correlation; in particular, the time lags at the peaks are nearly identical. We use a coincidence window of $\Delta t = 5$ ms, half of the typical burst width and half of the defined maximum interspike interval within bursts. The correlation is calculated for time lags over a ±1-s window.

From $K(\tau)$, we extract all peak values and their time lags τ. The significance of these peaks is assessed in relation to randomly shifted spike trains: both spike trains were divided into 500-ms windows, each of which was given a cyclic time shift randomly chosen in the range of 0 to 500 ms. (Sleep bursts tended to occur in epochs of 1 to 2 s; thus, shifting spike trains over intervals longer than 500 ms produces a weaker test of significance.) Peak values greater than zero were determined from 300 such randomized spike trains, typically yielding several thousand peaks. The distribution of peak values was used to find the 95% confidence level. Additional details on the computation of conditional correlations is described in the Supplementary Information.

Received 26 February; accepted 21 June 2002; doi:10.1038/nature00974.

1. Yu, A. C. & Margoliash, D. Temporal hierarchical control of singing in birds. *Science* **273,** 1871–1875 (1996).
2. Dave, A. S. & Margoliash, D. Song replay during sleep and computational rules for sensorimotor vocal learning. *Science* **290,** 812–816 (2000).
3. Nottebohm, F., Kelley, D. B. & Paton, J. A. Connections of vocal control nuclei in the canary telencephalon. *J. Comp. Neurol.* **207,** 344–357 (1982).
4. Scharff, C. & Nottebohm, F. A comparative study of the behavioral deficits following lesions of various parts of the zebra finch song system: implications for vocal learning. *J. Neurosci.* **11,** 2896–2913 (1991).
5. Barlow, H. *The Cognitive Neurosciences* 415–435 (MIT Press, Cambridge, Massachusetts, 1995).
6. Hermann, M., Hertz, J. & Prugel-Bennet, A. Analysis of synfire chains. *Network: Comput. Neural Syst.* **6(3),** 403–414 (1995).
7. Willshaw, D. J., Buneman, O. P. & Longuet-Higgins, H. C. Non-holographic associative memory. *Nature* **222,** 960–962 (1969).
8. Konishi, M. The role of auditory feedback in the control of vocalizations in the white-crowned sparrow. *Z. Tierpsychol.* **22,** 770–783 (1965).
9. Konishi, M. Birdsong: from behavior to neuron. *Ann. Rev. Neurosci.* **8,** 125–170 (1985).
10. Immelmann, K. in *Bird Vocalizations* (ed. Hinde, R. A.) 61–74 (Cambridge Univ. Press, New York, 1969).
11. Fee, M. S., Shraiman, B., Pesaran, B. & Mitra, P. P. The role of nonlinear dynamics of the syrinx in the vocalizations of a songbird. *Nature* **395,** 67–71 (1998).
12. Vu, E. T., Mazurek, M. E. & Kuo, Y. Identification of a forebrain motor programming network for the learned song of zebra finches. *J. Neurosci.* **14,** 6924–6934 (1994).
13. Vicario, D. S. Organization of the zebra finch song control system: II. Functional organization of outputs from nucleus robustus archistriatalis. *J. Comp. Neurol.* **309,** 486–494 (1991).
14. Wild, J. M. Descending projections of the songbird nucleus robustus archistriatalis. *J. Comp. Neurol.* **338,** 225–241 (1993).
15. Chi, Z. & Margoliash, D. Temporal precision and temporal drift in brain and behavior of zebra finch song. *Neuron* **32,** 899–910 (2001).
16. Doya, K. & Sejnowski, T. J. in *Central Auditory Processing and Neural Modeling* (eds Poon, P. W. F. & Brugge, J. F.) 77–88 (Plenum, New York, 1998).
17. Troyer, T. W. & Doupe, A. J. An associational model of birdsong sensorimotor learning II. Temporal hierarchies and the learning of song sequence. *J. Neurophysiol.* **84,** 1224–1239 (2000).
18. Mooney, R. Different subthreshold mechanisms underlie song selectivity in identified HVc neurons of the zebra finch. *J. Neurosci.* **201,** 5420–5436 (2000).
19. Dutar, P., Vu, H. M. & Perkel, D. J. Multiple cell types distinguished by physiological, pharmacological, and anatomic properties in nucleus HVc of the adult zebra finch. *J. Neurophysiol.* **80,** 1828–1838 (1998).
20. Swadlow, H. Neocortical efferent neurons with very slowly conducting axons: strategies for reliable antidromic identification. *J. Neurosci. Meth.* **79,** 131–141 (1998).
21. Brillinger, D. R., Bryant, H. L. & Segundo, J. P. Identification of synaptic interactions. *Biol. Cybernetics* **22,** 213–228 (1976).
22. Doupe, A. J. A neural circuit specialized for vocal learning. *Curr. Opin. Neurobiol.* **116,** 104–111 (1993).
23. Amari, S.-I. Learning patterns and pattern sequences by self-organizing nets of threshold elements. *IEEE Trans. Comput.* 1197–1206 (1972).
24. Kleinfeld, D. & Sompolinsky, H. in *Methods in Neuronal Modeling* (eds Koch, C. & Segev, I.) 195–246 (MIT Press, Cambridge, Massachusetts, 1989).
25. Pearlmutter, B. A. Learning state space trajectories in recurrent neural networks. *Neural Computat.* **1,** 263–269 (1989).
26. Bottjer, S. W., Halsema, K. A., Brown, S. A. & Miesner, E. A. Axonal connections of a forebrain nucleus involved with vocal learning in zebra finches. *J. Comp. Neurol.* **279,** 312–326 (1989).
27. Mooney, R. Synaptic basis for developmental plasticity in a birdsong nucleus. *J. Neurosci.* **12,** 2464–2477 (1992).
28. Brainard, M. S. & Doupe, A. J. Interruption of a basal ganglia-forebrain circuit prevents plasticity of learned vocalizations. *Nature* **404,** 762–766 (2000).
29. Phillips, N. H. & Berger, R. J. Melatonin infusions restore sleep suppressed by continuous bright light in pigeons. *Neurosci. Lett.* **145,** 217–220 (1992).
30. Fee, M. S. & Leonardo, A. Miniature motorized microdrive and commutator system for chronic neural recordings in small animals. *J. Neurosci. Meth.* **112,** 83–94 (2001).

Supplementary Information accompanies the paper on *Nature*'s website (http://www.nature.com/nature).

Acknowledgements

We acknowledge discussions with W. Denk, D. Lee, I. Nebel and S. Seung. We also thank F. Nottelbohm for comments on the manuscript. Recordings of RA neurons in the singing bird were carried out in collaboration with A. Leonardo. This work was supported in part by the National Science Foundation.

Competing interests statement

The authors declare that they have no competing financial interests.

Correspondence and requests for materials should be addressed to M.S.F. (e-mail: fee@lucent.com).

Deficient pheromone responses in mice lacking a cluster of vomeronasal receptor genes

Karina Del Punta*, Trese Leinders-Zufall†, Ivan Rodriguez*‡, David Jukam*, Charles J. Wysocki§, Sonoko Ogawa*, Frank Zufall† & Peter Mombaerts*

** The Rockefeller University, 1230 York Avenue, New York, New York 10021, USA*
† Department of Anatomy and Neurobiology and Program in Neuroscience, University of Maryland School of Medicine, Baltimore, Maryland 21201, USA
§ Monell Chemical Senses Center, 3500 Market Street, Philadelphia, Pennsylvania 19104, USA

The mammalian vomeronasal organ (VNO), a part of the olfactory system, detects pheromones—chemical signals that modulate social and reproductive behaviours[1,2]. But the molecular receptors in the VNO that detect these chemosensory stimuli remain undefined. Candidate pheromone receptors are encoded by two distinct and complex superfamilies of genes, *V1r* and *V2r* (refs 3 and 4), which code for receptors with seven transmembrane domains. These genes are selectively expressed in sensory neurons of the VNO. However, there is at present no functional evidence for a role of these genes in pheromone responses. Here, using chromosome engineering technology[5], we delete in the germ line of mice a ~600-kilobase genomic region that contains a cluster of 16 intact *V1r* genes[6]. These genes comprise two of the 12 described *V1r* gene families[7], and represent ~12% of the *V1r* repertoire. The mutant mice display deficits in a subset of VNO-dependent behaviours: the expression of male sexual behaviour and maternal aggression is substantially altered. Electrophysiologically, the epithelium of the VNO of such mice does not respond detectably to specific pheromonal ligands. The behavioural impairment and chemosensory deficit support a role of V1r receptors as pheromone receptors.

Vomeronasal sensory neurons (VSNs) in the mammalian VNO are thought to be specialized in the detection of pheromones[8,9], although their chemoreceptive abilities also extend to other types of ligands[10]. Much of our knowledge about mammalian VNO function has been obtained by describing the behavioural consequences of surgical lesions. Animals with complete anatomical removal of the VNO exhibit a range of deficits in social and reproductive behaviours, including the emission of male ultrasound vocalizations to females, intermale aggression, male sexual behaviour, and maternal aggression[11]. Pheromones, present in bodily secretions such as urine[1,2], elicit these VNO-dependent behaviours. *V1r* (ref. 3) and *V2r* (ref. 4) genes are proposed to encode candidate chemosensory receptors, specifically pheromone receptors, on the basis of predicted protein structure, patterns of expression, and genetic complexity. However, no ligands, natural or synthetic, are known for specific V1r or V2r receptors and there is no functional evidence implicating these receptors in pheromonal behaviours.

To determine if V1r receptors are involved in behavioural and electrophysiological responses to pheromones, we deleted a cluster of *V1r* genes in the germ line of mice. We[6] and others[12] have characterized the genomic organization of a cluster of *V1r* genes on chromosome 6. A ~600-kilobase (kb) region comprises 23 *V1r* genes of which 16 have an intact open reading frame (ORF); the remaining 7 *V1r* genes are pseudogenes, as their ORFs are disrupted. The mouse *V1r* superfamily[7] consists of ≥137 genes with an intact ORF that can be grouped into 12 phylogenetically highly isolated families (*V1ra-l*) (Fig. 1a). Our cluster represents ~12% of the potentially functional V1r repertoire, and contains most members of two *V1r* families, *V1ra* and *V1rb* (Fig. 1a, b), but no other genes[6,12]. To delete the gene cluster we used the technique of chromosome engineering[5], designed to excise large regions of genomic DNA via gene targeting and Cre-*loxP* mediated site-specific recombination in embryonic stem cells (Fig. 1b). The resulting homozygous mice, termed *ΔV1rabΔ* mice, harbour a ~600-kb genomic deletion and lack most *V1ra* and *V1rb* genes, as evidenced by Southern blot hybridization with a *V1ra/b* probe (Fig. 1c). One intact family member, *V1rb10*, located on the X chromosome[6], is not included in the deletion. *In situ* hybridization of the vomeronasal epithelium confirmed the expected absence of messenger RNA for the deleted *V1r* genes in the mutant mice (Fig. 1d). The expression of other families of *V1r* genes and the thickness of the layer of *V1r*-expressing VSNs are not obviously affected (Fig. 1d). The accessory olfactory bulb (AOB), which receives axonal input from VSNs, shows a normal overall size, layered organization, and rostral segregation of axons from VSNs expressing $G\alpha_{i2}$ (Fig. 1e, f).

Table 1 **VNO-independent functions**

	Genotype	
	WT	−/−
Weight		
Males (15-20 weeks) (g)	19.9 ± 3.3	19.0 ± 3.6
Females (17-19 weeks) (g)	16.0 ± 4.3	16.7 ± 4.4
Motor activity: bar hanging and balancing		
Time spent hanging on wire (s)	39.1 ± 7.6	41.9 ± 6.1
Time to right on wire (s)	2.8 ± 0.6	2.4 ± 0.5
Motor activity: screen climbing		
Time to climb to top of screen (s)	24.6 ± 2.8	26.7 ± 2.5
Locomotor activity in open field		
Total moving distance males (cm)	470.9 ± 93.2	456.8 ± 84.1
Total moving distance females (cm)	370.4 ± 85.6	422.2 ± 71.9
Depression-related behaviours		
Forced swim test (total immobility: min)	92.2 ± 14.4	84.3 ± 11.7
Tail suspension test (total immobility: min)	107.1 ± 5.6	109.2 ± 7.9
Oestrous cycling of females		
Mean number of cycles in 17 d	1.7 ± 0.1	1.8 ± 0.2
Olfactory function: latency to find cookie		
Day 1 (s)	218.3 ± 25.3	179.2 ± 25.9
Day 2 (s)	114.4 ± 20.6	89.9 ± 17.4
Day 3 (s)	86.0 ± 9.5	87.0 ± 10.3
Day 4 (s)	56.4 ± 6.4	58.3 ± 9.3

Body weight of males and females ($n = 30$ per genotype and sex), motor activity ($n = 20$ per genotype), locomotor activity ($n = 20$ per genotype and sex), depression-related behaviours ($n = 15$ per genotype and per test) and the number of oestrous cycles of non-group-housed females ($n = 15$ per genotype) were not significantly different between wild-type (WT) and mutant (−/−) mice as evaluated with an unpaired Student's *t*-test. The test of olfactory function was repeated over four consecutive days. Both genotypes learn to find the cookie faster with repeated trials. No significant differences were observed between the genotypes ($n = 15$ per genotype and sex), as evaluated with a two-way ANOVA for repeated measurements for main effects of genotype and test day and their interaction.

‡ Present address: Department of Zoology and Animal Biology, Faculty of Sciences, University of Geneva, CH-1211 Geneva 4, Switzerland.

alleles, their defective regulation by p107, and altered phosphorylation of the c-Myc transactivation domain. *Mol. Cell. Biol.* **15,** 4031–4042 (1995).
24. Eilers, M., Schirm, S. & Bishop, J. M. The MYC protein activates transcription of the α-prothymosin gene. *EMBO J.* **10,** 133–141 (1991).
25. Geiduschek, E. P. & Kassavetis, G. A. The RNA polymerase III transcription apparatus. *J. Mol. Biol.* **310,** 1–26 (2001).
26. Hateboer, G. *et al.* TATA-binding protein and the retinoblastoma gene product bind to overlapping epitopes on c-Myc and adenovirus E1A protein. *Proc. Natl Acad. Sci. USA* **90,** 8489–8493 (1993).
27. Cole, M. D. & McMahon, S. B. The Myc oncoprotein: a critical evaluation of transactivation and target gene regulation. *Oncogene* **18,** 2916–2924 (1999).
28. Eisenman, R. N. Deconstructing Myc. *Genes Dev.* **15,** 2023–2030 (2001).
29. Schübeler, D. *et al.* Nuclear localization and histone acetylation: a pathway for chromatin opening and transcriptional activation of the human β-globin locus. *Genes Dev.* **14,** 940–950 (2000).
30. White, R. J., Gottlieb, T. M., Downes, C. S. & Jackson, S. P. Mitotic regulation of a TATA-binding-protein-containing complex. *Mol. Cell. Biol.* **15,** 1983–1992 (1995).

Acknowledgements We thank C. Ngouenet and Z. Felton-Edkins for technical assistance, and R. Reeder, S. Cowley and C. Yost for critique of this manuscript. This work was funded by grants from CONACYT-Mexico (N.G.), the National Institutes of Health/National Cancer Institute (C.G. and R.N.E.), and from Cancer Research UK (R.J.W.).

Competing interests statement The authors declare that they have no competing financial interests.

Correspondence and requests for materials should be addressed to R.N.E. (e-mail: eisenman@fhcrc.org) or R.J.W. (e-mail: rwhite@udcf.gla.ac.uk).

errata

The role of parasites in sympatric and allopatric host diversification

Angus Buckling & Paul B. Rainey

Nature **420**, 496–499 (2002).

In Fig. 2b of this Letter, the third bar (dark grey) from the left was incorrectly shown. Its allopatric diversity value should have been 0.007 not 0.19. This error does not alter the conclusions of the paper. □

An ultra-sparse code underlies the generation of neural sequences in a songbird

Richard H. R. Hahnloser, Alexay A. Kozhevnikov & Michale S. Fee

Nature **419**, 65–70 (2002).

In this Letter, the numbering on the middle panel of Fig. 2b was misaligned. The figure should have appeared as shown.

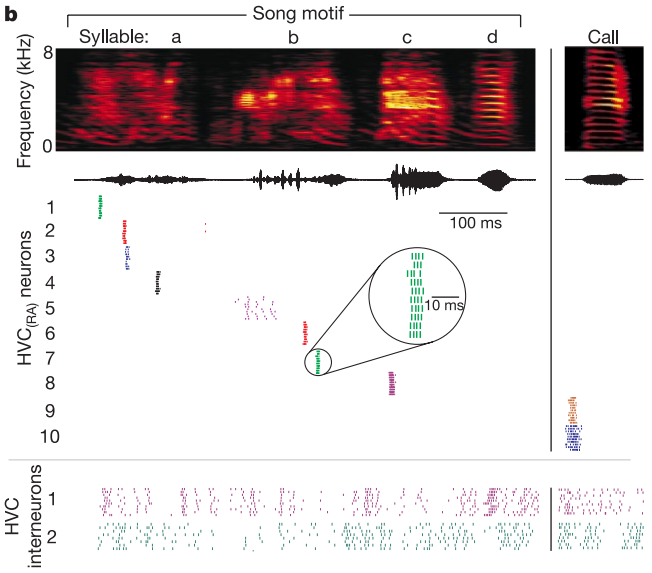

In the Acknowledgements, F. Nottebohm's surname was misspelled. □